



# Atomically thin layers of MoS<sub>2</sub> via a two step thermal evaporation-exfoliation method

Balendhran, Sivacarendran; Ou, Jian; Bhaskaran, Madhu; Sriram, Sharath; Ippolito, Samuel; Vasic, Zoran; Kats, Eugene

[https://researchrepository.rmit.edu.au/discovery/delivery/61RMIT\\_INST:ResearchRepository/12246640240001341?l#13248396600001341](https://researchrepository.rmit.edu.au/discovery/delivery/61RMIT_INST:ResearchRepository/12246640240001341?l#13248396600001341)

---

Balendhran, Ou, J., Bhaskaran, M., Sriram, S., Ippolito, S., Vasic, Z., Kats, E., Bhargava, S., Zhuiykov, S., & Kalantar Zadeh, K. (2012). Atomically thin layers of MoS<sub>2</sub> via a two step thermal evaporation-exfoliation method. *Nanoscale*, 4(2), 461–466. <https://doi.org/10.1039/c1nr10803d>

Document Version: Accepted Manuscript

---

Published Version: <https://doi.org/10.1039/c1nr10803d>

Repository homepage: <https://researchrepository.rmit.edu.au>

This journal is © The Royal Society of Chemistry 2012

Downloaded On 2022/08/05 01:55:33 +1000



**Thank you for downloading this document from the RMIT Research Repository.**

The RMIT Research Repository is an open access database showcasing the research outputs of RMIT University researchers.

RMIT Research Repository: <http://researchbank.rmit.edu.au/>

**Citation:**

Balendhran, S, Ou, J, Bhaskaran, M, Sriram, S, Ippolito, S, Vasic, Z, Kats, E, Bhargava, S, Zhuiykov, S and Kalantar Zadeh, K 2012, 'Atomically thin layers of MoS<sub>2</sub> via a two step thermal evaporation-exfoliation method', *Nanoscale*, vol. 4, no. 2, pp. 461-466.

See this record in the RMIT Research Repository at:

<http://researchbank.rmit.edu.au/view/rmit:14122>

Version: Accepted Manuscript

Copyright Statement: © This journal is © The Royal Society of Chemistry 2012

Link to Published Version:

<http://dx.doi.org/10.1039/c1nr10803d>

**PLEASE DO NOT REMOVE THIS PAGE**

# Atomically thin layers of MoS<sub>2</sub> via a two step thermal evaporation - exfoliation method

Sivacarendran Balendhran<sup>a\*</sup>, Jian Zhen Ou<sup>a</sup>, Madhu Bhaskaran<sup>a</sup>, Sharath Sriram<sup>a</sup>, Samuel Ippolito<sup>b</sup>, Zoran Vasic<sup>c</sup>, Eugene Kats<sup>d</sup>, Suresh Bhargava<sup>b</sup>, Serge Zhuiykov<sup>d</sup> and Kouros Kalantar-zadeh<sup>a\*</sup>

5 Received (in XXX, XXX) Xth XXXXXXXXXX 200X, Accepted Xth XXXXXXXXXX 200X

DOI: 10.1039/b000000x

Two dimensional molybdenum disulfide (MoS<sub>2</sub>) has recently become of interest of semiconductor and optic industries. However, the current methods for its synthesis require harsh environments that are not compatible with standard fabrication processes. We report on a facile synthesis method of layered MoS<sub>2</sub> using a thermal evaporation technique, which requires modest conditions. In this process, a mixture of MoS<sub>2</sub> and molybdenum dioxide (MoO<sub>2</sub>) is produced by evaporating sulphur powder and molybdenum trioxide (MoO<sub>3</sub>) nano-particles simultaneously. Further annealing in a sulphur-rich environment, transforms majority of the excess MoO<sub>2</sub> into layered MoS<sub>2</sub>. The deposited MoS<sub>2</sub> is then mechanically exfoliated into minimum resolvable atomically thin layers, which are characterized using micro Raman spectroscopy and atomic force microscopy. Furthermore Raman spectroscopy is employed to determine the effect of electrochemical lithium ion exposure on atomically thin layers of MoS<sub>2</sub>.

## Introduction

Since the breakthrough of graphene synthesis,<sup>1</sup> the physics of two dimensional (2D) materials has received increasing attention. Although graphene demonstrates excellent properties as a 2D conductive material, it is not the most viable in the realm of semiconductor physics as it does not possess a natural band gap. The presence of a band gap allows the material to switch on and off, which is a crucial property in electronic devices. It has been reported that a tunable band gap can be introduced in bi-layer graphene using a perpendicular electrical field,<sup>2</sup> along with reports of several other methods such as shaping graphene sheets into nano-ribbon forms.<sup>3</sup> Notwithstanding such reports, the band gap is in the order of a few hundred meV. Additionally, the processes for introducing a band gap in graphene are generally complex, resulting in crystallographic damage to the material and loss in desirable electrical properties such as electron mobility.<sup>4</sup> Hence, layered transition metal oxides and sulfides (such as MoO<sub>3</sub>, WO<sub>3</sub>, and MoS<sub>2</sub>) are promising and suitable candidates as 2D semiconducting materials due to their natural band gap. In the recent years, the synthesis of 2D materials based on MoO<sub>3</sub>,<sup>5</sup> WO<sub>3</sub>,<sup>6</sup> and MoS<sub>2</sub>,<sup>7,8</sup> using simple mechanical exfoliation has generated significant interest. Of these, MoS<sub>2</sub> is a more favorable material compared to transition metal oxides, since it has a relatively small band gap of 1.29 eV and 1.90 eV for the bulk material and single layers, respectively.<sup>9</sup> In addition MoS<sub>2</sub> is not fully saturated in sulphur, compared to MoO<sub>3</sub> and WO<sub>3</sub> which are in their maximum oxidation states.<sup>10</sup> Due to these characteristics, MoS<sub>2</sub> presents a wide range of applications such as mass-sensitive liquid pollutant sensors,<sup>10</sup> selective gas sensors,<sup>11</sup> catalysts,<sup>12</sup> hydrogen storages,<sup>13</sup> nano-lubricants,<sup>14-16</sup>

lithium ion battery anodes<sup>16,17</sup> and bio medical applications.<sup>18</sup>

The basic unit of MoS<sub>2</sub> is composed of a molybdenum atom coordinated with six sulphur atoms (Fig. 1). It is organized in two layers of sulphur atoms forming a sandwich structure, with a layer of molybdenum atoms in the middle. Each sulphur atom is coordinated with three molybdenum atoms within a single 2D layer of MoS<sub>2</sub>. The bulk material is formed of these 2D layers held together of van der Waals forces.<sup>19</sup> It has been demonstrated that these van der Waals forces are weak enough to let the material split into minimum resolvable atomic layers through mechanical<sup>7,9</sup> and liquid<sup>20,21</sup> exfoliation techniques. These atomically thin layers of MoS<sub>2</sub> display enhanced electrical and optical properties due to the quantum confinement effect.<sup>7</sup> Although the first measurements of carrier mobility in atomically thin layers of MoS<sub>2</sub> resulted in the observation of relatively small values in the range of 0.5-3.0 cm<sup>2</sup> V<sup>-1</sup> s<sup>-1</sup>,<sup>22</sup> Radisavljevic *et al.* have recently demonstrated the dramatic increase in electron mobility through a top gate approach in a field effect measurement. In this seminal work, by depositing a high dielectric material such as hafnium dioxide (HfO<sub>2</sub>) on atomically thin MoS<sub>2</sub>, mobility of ~217 cm<sup>2</sup> V<sup>-1</sup> s<sup>-1</sup> has been reported.<sup>7</sup> Such an increase in carrier mobility is of fundamental importance in electronic industry for the development of high gain and fast switching transistors. Splendiani *et al.* have also reported the transformation of MoS<sub>2</sub> band structure from indirect to direct band gap at 2D levels,<sup>8</sup> while demonstrating significant photoluminescence owing to this change in band structure.<sup>8,9</sup> Such a direct bandgap is also of elemental significance as it allows engineering novel optical behaviors and holds promise for new nanophotonic applications.

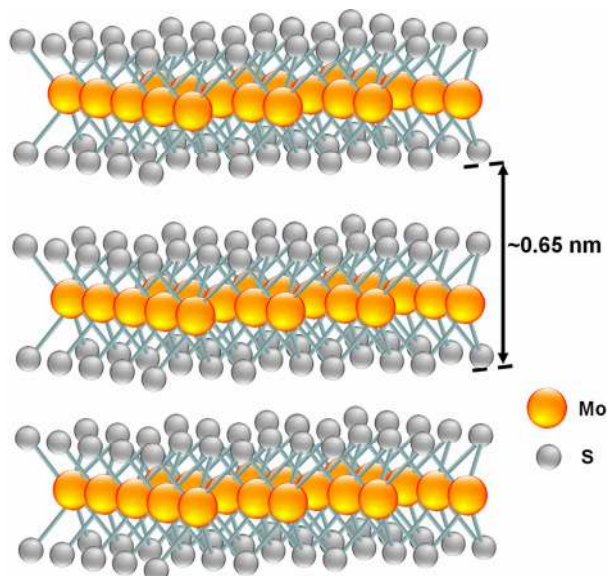


**Fig. 1** Visualization of the atomic structure of layered hexagonal MoS<sub>2</sub>.

The development of 2D materials is generally a two-step process: the synthesis of the layered bulk material followed by the exfoliation process.<sup>1, 6</sup> Although there is a wide range of controlled methods of synthesis available to produce different morphologies of MoS<sub>2</sub> such as hydrothermal,<sup>23</sup> solvothermal,<sup>24</sup> chemical transport reaction,<sup>25</sup> and high pressure-arc discharge,<sup>26</sup> synthesis of layered MoS<sub>2</sub> is a topic that is yet to be widely explored. A few known methods of layered MoS<sub>2</sub> synthesis are thermal decomposition of ammonium thiomolybdate precursors<sup>12</sup> and chemical reactions between sulphur and molybdenum based compounds.<sup>10, 27</sup> These methods consist of highly controlled parameters (pressure, temperature etc.), and also require complex chemical experimental apparatus (three zone furnace, autoclave setups etc.).<sup>25, 27, 28</sup> Some of these methods involve hazardous materials such as hydrogen sulfide (H<sub>2</sub>S) and carbon disulfide (CS<sub>2</sub>)<sup>12, 27</sup> and are also conducted over a long period of time<sup>27</sup> yield them unfavorable for applications in electronic and optical device fabrication industries.

One of the less explored methods for the fabrication of layered MoS<sub>2</sub> is thermal evaporation. Thermal evaporation in a horizontal furnace involves annealing commercially available materials containing molybdenum and sulphur at the required temperature in gaseous carriers.<sup>29</sup> Although this is a simple, fast and controllable process, thermal evaporation of commercial MoS<sub>2</sub> powder has so far not been considered since the evaporation temperature of MoS<sub>2</sub> is prohibitively high (1375 °C). In this work, we report a simple method of synthesis of layered MoS<sub>2</sub> through thermal evaporation of MoO<sub>3</sub> nano-powder along with excess sulphur, overcoming the direct evaporation barrier with MoS<sub>2</sub>. Additionally this approach does not produce hazardous gasses and also does not require complex experimental setups. The synthesis of MoS<sub>2</sub> by the co-evaporation process was carried out at various annealing temperatures and for different durations. The resulting thin films are then characterized using scanning electron microscopy (SEM), micro Raman spectroscopy, and X-ray diffraction (XRD) techniques. Mechanical exfoliation is conducted on the acquired samples and the flakes are analyzed using Raman spectroscopy and atomic

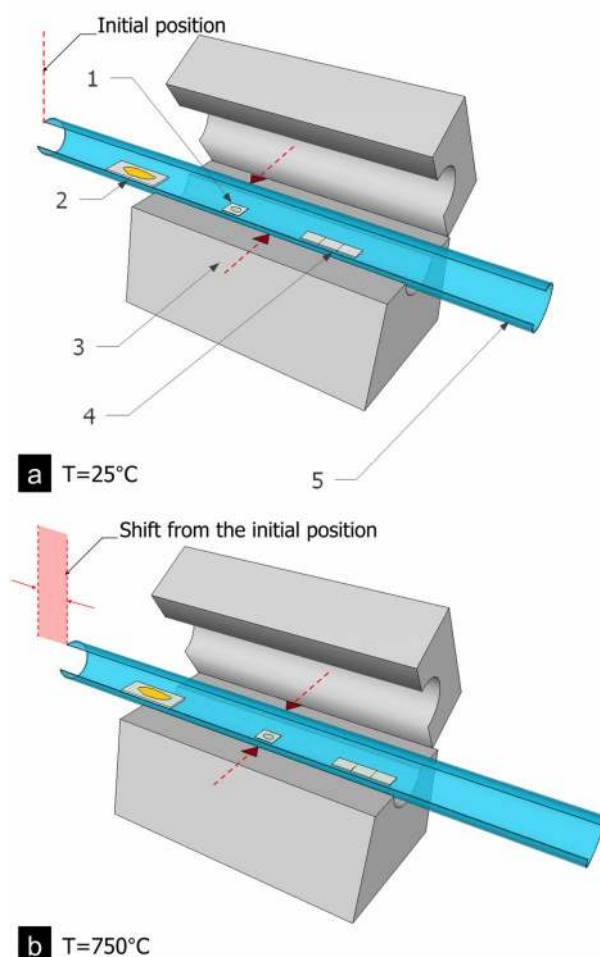


**Fig. 2** Experimental setup: (a) initially at room temperature, the centre of the tube is offset from the centre of the furnace and in (b) at 750°C, the tube is pushed inside the furnace aligning the centre of the tube with the centre of the furnace. Legend: (1) MoO<sub>3</sub> nano powder, (2) sulphur powder, (3) horizontal furnace, (4) quartz substrates for deposition and (5) quartz tube.

force microscopy (AFM). Lithium ion exposure studies of such layers are presented to demonstrate their unique properties in comparison to their thicker counterparts.

## Experimental

The thermal evaporation technique was applied in a horizontal furnace incorporating a quartz tube (Fig. 2). MoO<sub>3</sub> powder weighing 50 mg (99% purity, China Rare Material Company) was placed on a quartz substrate, which was then positioned in the center of the tube. Sulphur powder (99% purity, Sigma-Aldrich) was placed upstream relative to the gas flow direction, 20 cm from the MoO<sub>3</sub> powder. Quartz substrates were placed along the downstream side for the MoS<sub>2</sub> deposition.

The deposition process was conducted by evaporating sulphur powder and MoO<sub>3</sub> nano-particles simultaneously in an argon environment at a flow rate of 200 sccm. Further annealing was conducted in a sulphur rich environment to enhance the presence of MoS<sub>2</sub>. Initially, the center of the quartz tube was offset from the center of the furnace and was heated at a rate of 20 °C/min (Fig. 2a). As soon as the center of the furnace reached 750 °C the

quartz tube was pushed in (Fig. 2b), placing the center of the tube at the center of the furnace. This procedure allows the  $\text{MoO}_3$  and the sulphur to evaporate at the same time. Afterwards, the setup was held at the set temperature for the experimented annealing duration. The thermal evaporation process was carried out at different temperatures and durations in order to determine the optimal experimental conditions for layered  $\text{MoS}_2$  deposition. Three annealing conditions are presented in this work: (a) 775 °C for 60 mins, (b) 830 °C for 60 mins and (c) 830 °C for 180 mins. At the end of the process, the temperature was ramped down at 20 °C/min until room temperature was reached.

The obtained thin films were characterized using scanning electron microscopy, X-ray diffraction and Raman spectroscopy. SEM micrographs were acquired using a FEI Nova Nanoscope and the XRD diffractograms were obtained using a Bruker D8 microdiffractometer equipped with a general area detector diffraction system (GADDS). Data was collected at room temperature using a copper source with a potential of 40 kV and a current of 40 mA. The Raman measurements were performed over an accumulation time of 10 s for 3 accumulations using an Ocean Optics QE6500 spectrometer equipped with a 532 nm, 40 mW laser source.

In order to obtain thin layered  $\text{MoS}_2$ , adhesive tape was used on the deposited film to mechanically exfoliate the flakes<sup>5, 6</sup> and transfer them onto silica on silicon ( $\text{SiO}_2/\text{Si}$ ) substrates. Raman measurements on the exfoliated flakes were conducted over an accumulation time of 120 s for 2 accumulations using Jobin Yvon Horiba TRIAX 320 spectrometer equipped with a 532 nm,

0.7 mW laser source.

Atomic force microscopy was carried out on a Veeco Dimension Icon scanning probe microscope. For electrochemical ion intercalation, saturated lithium chloride ( $\text{LiCl}$ ) solution was prepared at room temperature. Mechanically exfoliated  $\text{MoS}_2$  flakes were transferred onto a conductive substrate (tungsten 25 nm on  $\text{SiO}_2/\text{Si}$  substrates) and Raman spectra was acquired for selected flakes. Platinum (Pt) foil was utilized as the anode and the conductive substrate containing the flakes as the cathode. Both the anode and cathode were completely submerged into the  $\text{LiCl}$  solution. A voltage of 4 V DC, for duration of 4 mins, was applied, allowing enough time for the intercalation process. The flakes were then located and Raman spectra were acquired to determine the effect of  $\text{Li}^+$  exposure.

## Results and Discussion

Micrographs of the deposited  $\text{MoS}_2$  thin films reveal the effect of the temperature and annealing duration on surface morphology. Fig. 3a shows the film obtained by annealing at 775 °C for 60 mins. The film does not have a well-defined structure. The magnified view of the surfaces and the blunt edges of these crystals indicates the possibility of rather amorphous growth achieved at lower temperatures. The increase in the temperature (830 °C) for the same annealing duration seems to have shifted the crystal growth towards layered structures. Fig. 3b illustrates these smooth surfaces and refined edges of the morphology acquired at 830 °C. Fig. 3c provides a view of the general surface morphology of the deposition achieved by further increasing the annealing duration to 180 mins at 830 °C. The surface proves to be a collection of randomly stacked micro platelets. These layered platelets seem to have average side lengths of a few micrometers. Well defined flakes with sharp edges and smooth layered surfaces have been produced, as shown on Fig. 3d. The thicknesses of these structures have been observed to be around 30 nm or lesser (Fig. 3e).

Raman spectroscopy was carried out to analyze the bond symmetry in the deposited thin films. In all three cases, Raman peaks corresponding to  $\text{MoS}_2$  were observed (Fig. 4). The vibration of Mo-S bond ( $E_{2g}^1$ ) along the base plane was observed at 381  $\text{cm}^{-1}$  and vibration of sulphur along the vertical ( $A_{1g}$ ) axis was observed at 406  $\text{cm}^{-1}$ .<sup>19, 25</sup> For the deposition at 775 °C for 60 mins, broad  $\text{MoS}_2$  peaks were observed (Fig. 4a). As the annealing temperature was increased to 830 °C for the same annealing duration, the spectra reveal better defined peaks (Fig. 4b) in comparison with the samples acquired at lower temperatures. By increasing the annealing duration from 60 mins to 180 mins, well-defined narrow peaks were observed at 830 °C (Fig. 4c). Also observed were weak peaks corresponding to  $\text{MoO}_2$ . Based on these observations, for temperatures less than 775 °C, the deposited film is nanocrystalline and as the temperature increases to 830 °C a more crystalline  $\text{MoS}_2$  is obtained. As the annealing duration was further increased to 180 mins, the observed narrow Raman peaks indicate the presence of highly-ordered layered structures. Raman spectroscopy results concur with the surface morphologies observed in the SEM micrographs (Fig. 3).

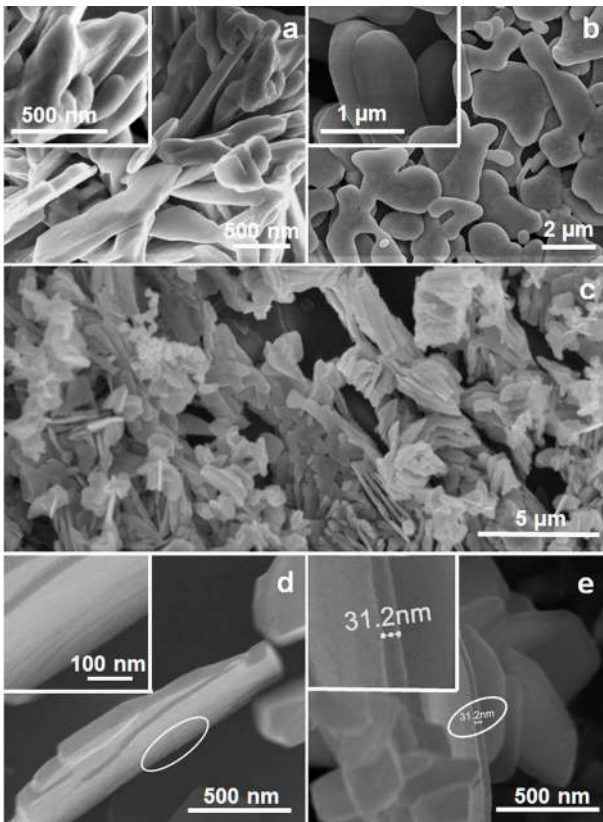


**Fig. 3** Scanning electron micrographs of the  $\text{MoS}_2$  deposition on quartz substrates obtained by thermal evaporation and annealed at: (a) 775 °C for 60 mins, (b) 830 °C for 60 mins, and (c-e) 830 °C for 180 mins.

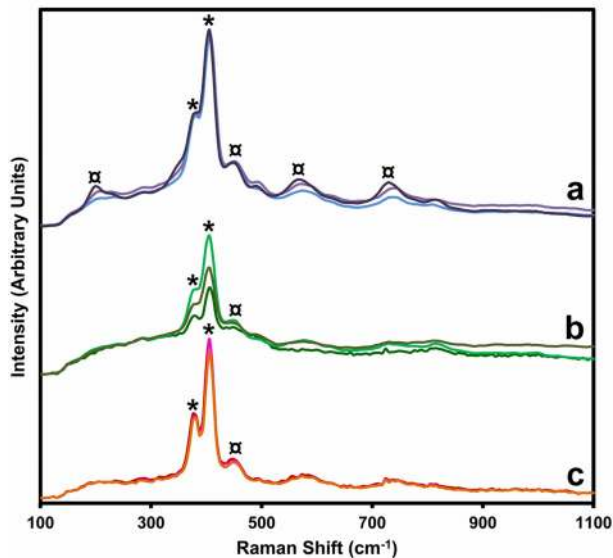


**Fig. 4** Raman spectra of MoS<sub>2</sub> deposition on quartz substrates: (a) annealed at 775 °C for 60 mins, (b) annealed at 830 °C for 60 mins, and (c) annealed at 830 °C for 180 mins (peaks correspond to [\*]MoS<sub>2</sub> and [□]MoO<sub>2</sub>).

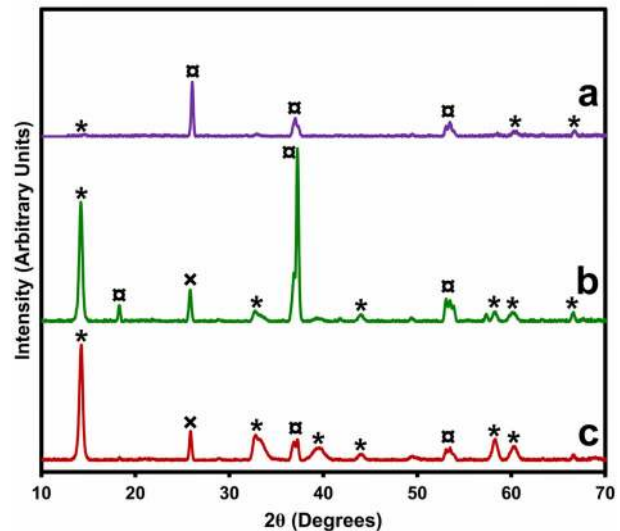


**Fig.5** XRD patterns of MoS<sub>2</sub> deposition on quartz substrates: (a) annealed at 775 °C for 60 mins, (b) annealed at 830 °C for 60 mins, and (c) annealed at 830 °C for 180 mins (peaks correspond to [\*]MoS<sub>2</sub>, [□]MoO<sub>2</sub> and [x]MoO<sub>3</sub>). The results display the progress of MoS<sub>2</sub> formation from MoO<sub>2</sub> in correspondence with temperature and time.

XRD was used to study the crystal structure of the deposited thin films. The XRD pattern of the as-deposited samples annealed at 775 °C for 60 minutes (Fig. 5a), reflect the dominant peak at 2θ of 26.08° corresponding to (011) plane of MoO<sub>2</sub> (ICDD Card No: 76-1807). Secondary peaks at 37.4°, 53.3°, and 53.6° corresponding to MoO<sub>2</sub> were also observed. Peaks corresponding to MoS<sub>2</sub> could be barely resolved. When temperature increased to 830 °C however for smaller annealing duration, the dominant peak was observed at 37.4° corresponding to (002) plane of layered hexagonal MoS<sub>2</sub> at 14.4° (ICDD Card No: 77-1716) was also observed. The MoS<sub>2</sub> peaks appeared in intensities significantly larger than the deposition achieved in the lower temperature case. In addition, a peak corresponding to (001) plane of MoO<sub>2</sub> was observed at 18.4° indicating better crystallinity in comparison with the film obtained at 775°C. For the sample annealed at 830 °C for 180 mins, the intensity of (002) MoO<sub>2</sub> peak was significantly lower with the (002) MoS<sub>2</sub> peak emerging as the dominant peak indicating larger presence of ordered MoS<sub>2</sub> (Fig. 5c). This spectrum shows the dominant presence of well-stacked, highly crystalline 2H-MoS<sub>2</sub>. The peaks at 32.7°, 33.5°, and 58.3° correspond to (100), (101), and (110) planes of 2H-MoS<sub>2</sub>, respectively. In this case, intensities of all MoO<sub>2</sub> peaks have significantly reduced in contrast to the MoS<sub>2</sub> peaks, indicating that the film has dominantly transformed into MoS<sub>2</sub>. Peaks corresponding to MoO<sub>3</sub> were observed in the case of the higher temperature process. We believe that at this temperature sulphur replaces oxygen in MoO<sub>2</sub> to form MoS<sub>2</sub>. The released oxygen ions at higher temperatures along with the lack of gaseous sulphur contribute to the re-oxidation of a fraction of MoO<sub>2</sub> to MoO<sub>3</sub>. Similar observation has been reported by Ressler *et al.* in a study of H<sub>2</sub> based reduction of MoO<sub>3</sub>.<sup>30</sup> Further discussion can be found in the Electronic Supplementary Information. Based on the collective observation, it is apparent that at lower synthesis temperatures, the concentration of MoS<sub>2</sub> in the films is significantly lower than MoO<sub>2</sub>. At the increased

temperatures of 830 °C, a combination of crystalline MoS<sub>2</sub> and MoO<sub>2</sub> deposition is obtained. With the increase of annealing duration at 830 °C, the presence of MoO<sub>2</sub> is significantly reduced and dominantly MoS<sub>2</sub> is achieved. From these experiments, it can be concluded that the reaction occurs in two phases; phase one involves sulphur vapor reducing MoO<sub>3</sub> to MoO<sub>2</sub> and in the second phase the excess sulphur reacts with MoO<sub>2</sub> and produces MoS<sub>2</sub>. The process temperature and reaction duration determine the degree of conversion of the original MoO<sub>3</sub> powder into a thermally evaporated MoS<sub>2</sub> film.

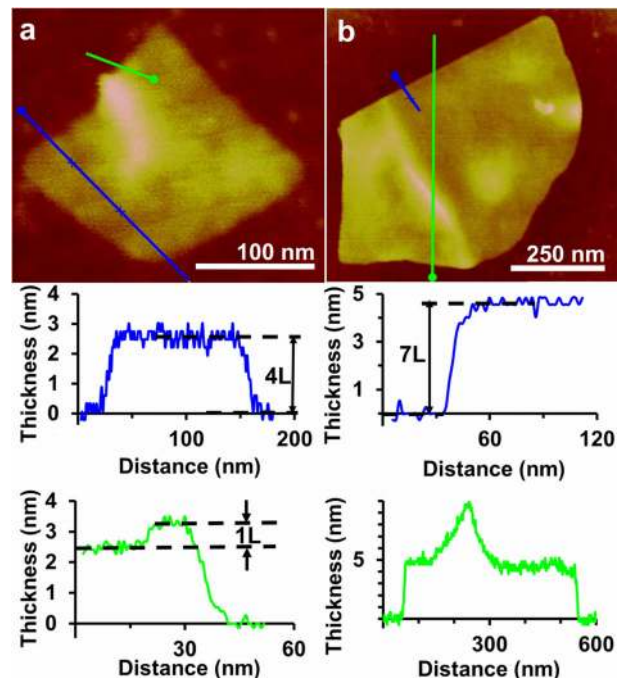


**Fig. 6** AFM scans of two different MoS<sub>2</sub> flakes exfoliated on SiO<sub>2</sub>/Si substrates and their corresponding cross sectional thicknesses: (a) Flake consisting of clearly resolved single step on its surface and (b) a large flake made of 7 layers showing a slightly folded structure.

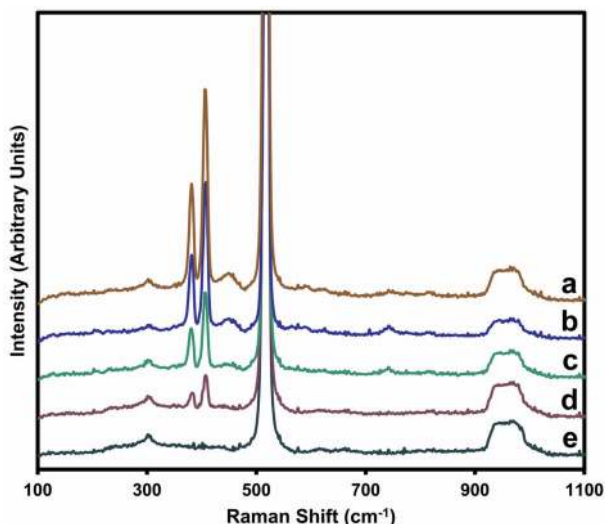


**Fig. 7** Raman spectra of (a-d) exfoliated MoS<sub>2</sub> flakes with thickness reducing from (a) to (d) in a range of 50 nm to 5 nm and (e) background substrate SiO<sub>2</sub>/Si.

5 Mechanical exfoliation was conducted on the samples evaporated at 830 °C and annealed for 180 mins, which was dominantly MoS<sub>2</sub>. Atomic force microscopy was used to determine the thickness and the presence of a layered structure in the exfoliated flakes. The thickness analysis through atomic  
 10 microscopy reveals flakes with typical thicknesses ranging from 5 to 50 nm. The atomic force microscopy results also concur that the exfoliated flakes are indeed layered (Fig. 6). Fig. 6a illustrates a random MoS<sub>2</sub> flake mainly consisting of four fundamental atomic layers. Cross sectional profiling also shows that some  
 15 parts of the flake consists of several more layers that are stacked on its surface. A step of ~0.65 nm can be clearly resolved in Fig. 6a, which corresponds to the fundamental thickness of a single atomic layer of MoS<sub>2</sub><sup>7</sup>. Additionally, a MoS<sub>2</sub> flake consisting of approximately seven layers can be seen in Fig 6b.  
 20 Interestingly, surface bulges and folds can be recognized in the image. This indicates that a few layers of MoS<sub>2</sub> can be flexible enough to be bent without breaking, similar to graphene sheets.<sup>31</sup> Additional cross sectional AFM scans are available in the Electronic Supplementary Information.

25 Micro Raman spectroscopy was employed for characterizing the exfoliated flakes as it has been proven to be an excellent tool for assessing 2D materials, which are obtained via the exfoliation method.<sup>1, 22</sup> Raman spectra of randomly exfoliated flakes of different thicknesses were obtained in order to determine their  
 30 composition. Spectra of the exfoliated flakes with thicknesses reducing from 50 to 5 nm are presented in Fig. 7a to Fig. 7d. The obtained spectra reveal vibration modes for the flakes identical to the as-deposited MoS<sub>2</sub> films with no MoO<sub>2</sub> contamination with reducing thickness. This suggests that the top surface of the  
 35 synthesized films is dominantly MoS<sub>2</sub> and the observed MoO<sub>2</sub> contribution in the X-ray diffractograms is mainly from the bottom of the films. The strong peak at 521 cm<sup>-1</sup> and the other weak features around 300, 900-1000 cm<sup>-1</sup> in the spectra correspond to the silica on silicon substrate, and is verified by a  
 40 background spectral measurement (Fig. 7e).

Raman spectroscopy was used to characterize the effect of lithium ion (Li<sup>+</sup>) exposure for two exfoliated flakes of different

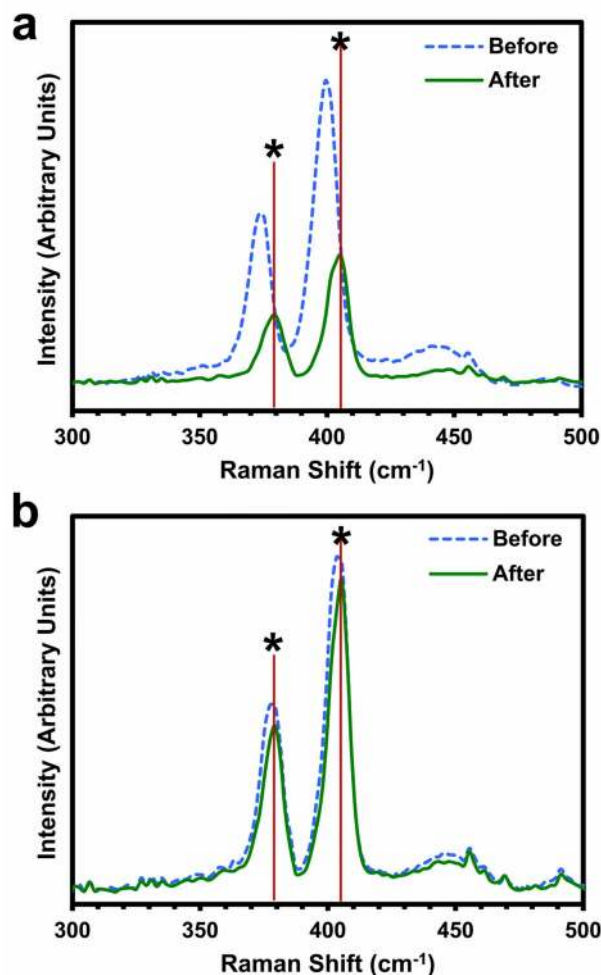


**Fig. 8** Raman spectra acquired before and after Li<sup>+</sup> intercalation of two different MoS<sub>2</sub> flakes: (a) thickness ~10 nm and (b) thickness >20 nm. [\*] represent the MoS<sub>2</sub> peak locations corresponding to the as deposited thin films.

thicknesses. Fig. 8 shows the Raman spectrum acquired before and after Li<sup>+</sup> exposure of two randomly targeted flakes. Lee *et al.*  
 50 reported the shift of Raman peaks for E<sub>2g</sub><sup>1</sup> and A<sub>1g</sub> at a level of few atomic layers<sup>32</sup> in comparison with the bulk material. This can be observed in Fig. 8: the spectra for flakes in Fig. 8a (thickness ~10 nm) and in Fig. 8b (thickness >20 nm) both show a shift in E<sub>2g</sub><sup>1</sup> and A<sub>1g</sub> modes before the intercalation with respect  
 55 to the bulk material. For both flakes, after the Li<sup>+</sup> exposure the peak shift is observed to the right with respect to the initial Raman spectra before the exposure. The shift observed in the Raman spectra can be related to a strain introduced into these bonds, which is due to the interstitial occupation by Li<sup>+</sup>.<sup>33</sup>  
 60 However as observed, the shift is significantly larger for the thinner flake. This can be due to a better efficiency for the intercalation of the the Li<sup>+</sup>, when the number of layers is reduced. In addition, a significant reduction in the intensity of the Raman spectrum can also be observed for the thin flake. This is in  
 65 agreement with the report by Julien *et al.*, who also observed similar reductions for bulk MoS<sub>2</sub>.<sup>33</sup> which they ascribed to the mild Li<sup>+</sup> intercalation forming Li<sub>0.1</sub>MoS<sub>2</sub>. More detailed Raman spectroscopy based studies for Li<sup>+</sup> intercalation of thin layered MoS<sub>2</sub> is to be undertaken in future work.

## Conclusion

We have demonstrated the successful synthesis of layered hexagonal MoS<sub>2</sub>, through a simple method of thermal evaporation in a reduction environment. This method uses temperatures less than 830 °C which is much less than the temperature, which is required for the direct evaporation of MoS<sub>2</sub>. By the application of mechanical exfoliation technique on the layered MoS<sub>2</sub>, we have obtained atomically thin layers of MoS<sub>2</sub> with the steps of ~0.65 nm corresponding to the fundamental thickness of the material. These atomically thin layers can be utilized in the fabrication of electronic devices of high carrier mobility to pave the way into the next generation of electronic devices.

## Acknowledgements

MB and SS acknowledge the Australian Post-Doctoral Fellowships from the Australian Research Council through Discovery Projects DP1092717 and DP110100262, respectively. SS and KKZ acknowledge the Australian Research Council for equipment funding through the Linkage, Infrastructure, Equipment, and Facilities Grant LE100100215. The work was partially supported by the CSIRO Sensors and Sensor Networks Transformational Capability Platform and CSIRO Materials Science and Engineering Division – strategic co-investment SIP6 project “Tiny Scale Sensors Networks”.

## Notes and references

<sup>a</sup>School of Electrical and Computer Engineering, RMIT University, Melbourne, VIC, Australia; E-mail: [shiva.balendhran@rmit.edu.au](mailto:shiva.balendhran@rmit.edu.au) and [kouros.kalantar@rmit.edu.au](mailto:kouros.kalantar@rmit.edu.au)

<sup>b</sup>School of Applied Sciences, RMIT University, Melbourne, VIC, Australia

<sup>c</sup>Melbourne Centre for Nano Fabrication, Clayton, VIC, Australia

<sup>d</sup>Materials Science and Engineering Division, CSIRO, Highett, VIC, Australia

† Electronic Supplementary Information (ESI) available: Further AFM scans and a discussion on the reaction mechanisms are included. See DOI: 10.1039/b000000x/

1. K. S. Novoselov, A. K. Geim, S. V. Morozov, D. Jiang, Y. Zhang, S. V. Dubonos, I. V. Grigorieva and A. A. Firsov, *Science*, 2004, **306**, 666–669.
2. Y. Zhang, T.-T. Tang, C. Girit, Z. Hao, M. C. Martin, A. Zettl, M. F. Crommie, Y. R. Shen and F. Wang, *Nature*, 2009, **459**, 820–823.
3. M. Y. Han, B. Ozyilmaz, Y. B. Zhang and P. Kim, *Phys. Rev. Lett.*, 2007, **98**, 206805.
4. X. L. Li, X. R. Wang, L. Zhang, S. W. Lee and H. J. Dai, *Science*, 2008, **319**, 1229–1232.
5. K. Kalantar-zadeh, A. Vijayaraghavan, M. H. Ham, H. D. Zheng, M. Breedon and M. S. Strano, *Chem. Mater.*, 2010, **22**, 5660–5666.
6. K. Kalantar-zadeh, J. S. Tang, M. S. Wang, K. L. Wang, A. Shailos, K. Galatsis, R. Kojima, V. Strong, A. Lech, W. Wlodarski and R. B. Kaner, *Nanoscale*, 2010, **2**, 429–433.
7. B. Radisavljevic, A. Radenovic, J. Brivio, V. Giacometti and A. Kis, *Nat. Nanotechnol.*, 2011, **6**, 147–150.
8. A. Splendiani, L. Sun, Y. B. Zhang, T. S. Li, J. Kim, C. Y. Chim, G. Galli and F. Wang, *Nano Lett.*, 2010, **10**, 1271–1275.
9. K. F. Mak, C. Lee, J. Hone, J. Shan and T. F. Heinz, *Phys. Rev. Lett.*, 2010, **105**, 136805.
10. P. A. Lieberzeit, A. Aftal, A. Rehman and F. L. Dickert, *Sensor. Actuat. B–Chem.*, 2007, **127**, 132–136.
11. B. K. Miremedi, R. C. Singh, S. R. Morrison and K. Colbow, *Appl. Phys. A–Mater.*, 1996, **63**, 271–275.
12. H. Farag, A. N. A. El-Hendawy, K. Sakanishi, M. Kishida and I. Mochida, *Appl. Catal. B–Environ.*, 2009, **91**, 189–197.
13. J. Chen and F. Wu, *Appl. Phys. A–Mater.*, 2004, **78**, 989–994.
14. V. N. Bakunin, A. Y. Suslov, G. N. Kuzmina, O. P. Parenago and A. V. Topchiev, *J. Nanopart. Res.*, 2004, **6**, 273–284.
15. C. Lee, Q. Y. Li, W. Kalb, X. Z. Liu, H. Berger, R. W. Carpick and J. Hone, *Science*, 2010, **328**, 76–80.
16. J. Xiao, D. W. Choi, L. Cosimbescu, P. Koech, J. Liu and J. P. Lemmon, *Chem. Mater.*, 2010, **22**, 4522–4524.
17. K. Chang, W. Chen, L. Ma, H. Li, H. Li, F. Huang, Z. Xu, Q. Zhang and J.-Y. Lee, *J. Mater. Chem.*, 2011, **21**, 6251–6257.
18. H. H. Wu, R. Yang, B. M. Song, Q. S. Han, J. Y. Li, Y. Zhang, Y. Fang, R. Tenne and C. Wang, *ACS Nano*, 2011, **5**, 1276–1281.
19. T. J. Wieting and J. L. Verble, *Phys. Rev. B*, 1971, **3**, 4286–4292.
20. A. S. Golub, D. P. Rupasov, N. D. Lenenko and Y. N. Novikov, *Russ. J. Inorg. Chem.*, 2010, **55**, 1166–1171.
21. J. N. Coleman, M. Lotya, A. O’Neill, S. D. Bergin, P. J. King, U. Khan, K. Young, A. Gaucher, S. De, R. J. Smith, I. V. Shvets, S. K. Arora, G. Stanton, H. Y. Kim, K. Lee, G. T. Kim, G. S. Duesberg, T. Hallam, J. J. Boland, J. J. Wang, J. F. Donegan, J. C. Grunlan, G. Moriarty, A. Shmeliov, R. J. Nicholls, J. M. Perkins, E. M. Grievson, K. Theuwissen, D. W. McComb, P. D. Nellist and V. Nicolosi, *Science*, 2011, **331**, 568–571.
22. K. S. Novoselov, D. Jiang, F. Schedin, T. J. Booth, V. V. Khotkevich, S. V. Morozov and A. K. Geim, *Proc. Natl. Acad. Sci. U. S. A.*, 2005, **102**, 10451–10453.
23. Y. Tian, Y. He and Y. Zhu, *Chem. Lett.*, 2003, **32**, 768–769.
24. D. Duphil, S. Bastide and C. Levy-Clement, *J. Mater. Chem.*, 2002, **12**, 2430–2432.
25. M. Virsek, M. Krause, A. Kolitsch and M. Remskar, *Phys. Status Solidi B*, 2009, **246**, 2782–2785.
26. M. Chhowalla and G. A. J. Amaratunga, *Nature*, 2000, **407**, 164–167.
27. X. Y. Chen, X. Wang, Z. H. Wang, W. C. Yu and Y. T. Qian, *Mater. Chem. Phys.*, 2004, **87**, 327–331.
28. G. W. Li, C. S. Li, H. Tang, K. S. Cao, J. A. Chen, F. F. Wang and Y. Jin, *J. Alloy. Compd.*, 2010, **501**, 275–281.
29. X. L. Li and Y. D. Li, *Chem. –Euro. J.*, 2003, **9**, 2726–2731.
30. T. Ressler, R. E. Jentoft, J. Wienold, M. M. Gunter and O. Timpe, *J. Phys. Chem. B*, 2000, **104**, 6360–6370.
31. X. Q. Zhang, S. H. Wan, J. B. Pu, L. P. Wang and X. Q. Liu, *J. Mat. Chem.*, 2011, **21**, 12251–12258.
32. C. Lee, H. Yan, L. E. Brus, T. F. Heinz, J. Hone and S. Ryu, *ACS Nano*, 2010, **4**, 2695–2700.
33. C. Julien, T. Sekine and M. Balkanski, *Solid State Ion.*, 1991, **48**, 225–229.